JOURNAL OF GUIDANCE, CONTROL, AND DYNAMICS
Vol. 34, No. 4, July–August 2011

Wind Field Estimation for Small Unmanned Aerial Vehicles

Jack W. Langelaan*
Pennsylvania State University, University Park, Pennsylvania 16802
and
Nicholas Alley† and James Neidhoefer‡
Area-I, Inc., Canton, Georgia 30115

DOI: 10.2514/1.52532

This paper describes a method for estimating wind field (wind velocity, rate of change of wind velocity, and wind gradient) for small and mini unmanned aerial vehicles. The approach uses sensors that are already part of a standard autopilot sensor suite (Global Positioning System, inertial measurement unit, airspeed, and magnetometer). The primary motivation is enabling energy harvesting; a secondary motivation is development of a low-cost atmospheric measurement and sampling system. The paper presents an error analysis and discusses the primary contributions to error in the estimated wind field. Results of Monte Carlo simulations compare predicted errors in wind estimates with actual errors and show the effect of using estimated winds for energy harvesting from gusts.

Nomenclature

$\mathbf{b}$	=	bias vector
$\mathbf{g}$	=	gravity vector
$\mathbf{H}$	=	Jacobian of measurement equation
h	=	measurement equation or altitude
$\mathbf{i}$, $\mathbf{j}$, $\mathbf{k}$	=	unit vectors
L	=	gust length scale
m	=	mass
$\mathbf{n}$	=	noise vector
p, q, r	=	components of body angular rate
$\mathbf{r}$	=	position in inertial frame
$\mathbf{T}$	=	direction cosine matrix
t	=	time
u, v, w	=	components of velocity with respect to air mass (expressed in body frame)
$\mathbf{v}_a$	=	velocity with respect to air mass
$\mathbf{w}$	=	wind vector
$\mathbf{X}$, $\mathbf{Y}$, $\mathbf{Z}$	=	aerodynamic forces
$\mathbf{x}$	=	state vector
x, y, z	=	position coordinates
$\mathbf{z}$	=	measurement vector
α	=	angle of attack
β	=	angle of sideslip
γ	=	flight-path angle with respect to air mass
$\mathbf{\Sigma}$	=	noise covariance matrix
σ	=	component of noise covariance or gust intensity
Φ	=	gust power spectral density
ϕ, θ, ψ	=	Euler angles
φ	=	phase
Ω	=	gust spatial frequency
$\boldsymbol{\omega}$	=	aircraft angular rate vector

Subscripts

b	=	body frame components
i	=	inertial frame components
imu	=	inertial measurement unit
k	=	time index
w	=	wind

Presented as Paper 2010-8177 at the AIAA Guidance, Navigation and Control Conference, Toronto, Ontario, Canada, 2–5 August 2010; received 24 September 2010; revision received 17 January 2011; accepted for publication 17 January 2011.

*Assistant Professor, Department of Aerospace Engineering. Associate Fellow AIAA.
†Member AIAA.
‡Associate Fellow AIAA.

I. Introduction

INTEREST in the problem of autonomous atmospheric energy harvesting (i.e., autonomous soaring) has been growing over the past few years. Observations of bird flight published by Rayleigh in 1883 and 1889 [1,2] provided early indications of the potential for energy harvesting using appropriate flight techniques. More recent work by Pennycuick [3] and Sachs [4] quantified the conditions under which birds such as albatrosses are able to harvest energy from spatial gradients in the wind field.

Knowledge of wind field is generally implicitly assumed in autonomous energy harvesting research. Dynamic soaring typically assumes full a priori knowledge of the wind field and casts energy harvesting as a trajectory optimization problem [5,6], and even gust soaring assumes knowledge of current wind conditions [7,8].

This paper is concerned with estimating wind conditions to enable gust soaring. Since the motivation is small low-cost unmanned aerial vehicles (UAVs) (here, small is assumed to mean hand-launchable vehicles ranging from 1 kg mass/1 m span to 10 kg mass/4 m span), minimizing sensing requirements is a priority. For example, while accurate measurements of wind field (including spatial gradients) can be obtained using arrays of multihole pitot probes [9], the intent here is to obtain estimates of wind field using only sensing that is already available on the aircraft. This sensing suite (included in typical autopilot modules) includes the Global Positioning System (GPS), an inertial measurement unit (IMU), a magnetometer, static pressure, and dynamic pressure. It is further assumed that the autopilot module computes an estimate of aircraft state (position, orientation, and velocity with respect to the Earth and velocity with respect to the air mass). Position and velocity are assumed to be available at a high rate (50 Hz) through fusion of GPS and inertial measurements. Note that the estimate of state is not assumed to be perfect: this paper also discusses the effect of noise and errors in the aircraft state estimate on the computed wind field.

Dynamic soaring and efficient gust soaring can, under certain conditions, make significant use of gradients and rates of change of the wind field. Hence, the wind estimation system should be able to obtain estimates of gradients and rates of change of wind velocity as well as the components of wind velocity.

A significant amount of research has been conducted for wind estimation. Pachter et al. uses GPS inertial and air data measurements to estimate horizontal components of windspeed and vehicle heading angle, but they did not address wind gradients or acceleration [10]. Rodriguez et al. used GPS, air data, and optical flow to compute windspeed for planar flight [11]. Myschik et al. [12] and Myschik and

Sachs [13] discussed an integrated wind estimation/navigation system for use on general aviation aircraft. De Divitiis described a variational technique for wind estimation for a small ducted fan vehicle [14].

II. Wind Estimation

A. Wind Field

Wind is assumed to be a spatially and temporally varying vector field:

$$\mathbf{w}(x, y, z, t) = \begin{bmatrix} w_{i,x}(x, y, z, t) \\ w_{i,y}(x, y, z, t) \\ w_{i,z}(x, y, z, t) \end{bmatrix} \tag{1}$$

A vehicle flying through this field is influenced by the components of the wind field, local temporal variations of the wind field, and gradients of the wind field. The rate of change of wind velocity, as seen by the vehicle, is a function of the rate of change of windspeed at a point, the field gradient, and the vehicle velocity:

$$\frac{\mathrm{d}}{\mathrm{d}t}\mathbf{w}(x, y, z) = \begin{bmatrix} \dot{w}_{i,x} \\ \dot{w}_{i,y} \\ \dot{w}_{i,z} \end{bmatrix} = \begin{bmatrix} \dot{w}^l_{i,x} \\ \dot{w}^l_{i,y} \\ \dot{w}^l_{i,z} \end{bmatrix} + \nabla\mathbf{w} \begin{bmatrix} \dot{x} \\ \dot{y} \\ \dot{z} \end{bmatrix} \tag{2}$$

Here, $\dot{x}$, $\dot{y}$, and $\dot{z}$ are the components of the velocity of the vehicle with respect to the inertial frame and $\nabla\mathbf{w}$ is the spatial gradient of the wind field. The superscript l denotes the time rate of change of wind velocity at the point (x, y, z). For a frozen wind field, this is zero; however, the approximation of a frozen wind field is only applicable when vehicle velocity is large compared with the point rates of change of wind velocity.

Unless arrays of air data probes are used, separating the effect of gradients from the point rates of change is extremely difficult without making several approximations and simplifications. MIL-F-8785C [15] suggests treating wind gradients as equivalent to aircraft angular velocities, with

$$p_w = -\frac{\delta w_{b,z}}{\delta y} \tag{3}$$

$$q_w = \frac{\delta w_{b,z}}{\delta x} \tag{4}$$

$$r_w = \frac{\delta w_{b,y}}{\delta x} \tag{5}$$

where the subscript b denotes components of wind expressed in the body frame [15].

This definition assumes that the effects of some components of gradient are negligible because of typical aircraft configuration: for example, wing span is significantly larger than tail height, so vertical gradient of the lateral air mass velocity has negligible effect on roll rate.

Depending on the ultimate application of the wind field estimates, it may be unnecessary to separate the effect of point changes in windspeed from the effect of gradients. This paper will focus on the problem of estimating the velocity vector and the net rate of change of wind velocity.

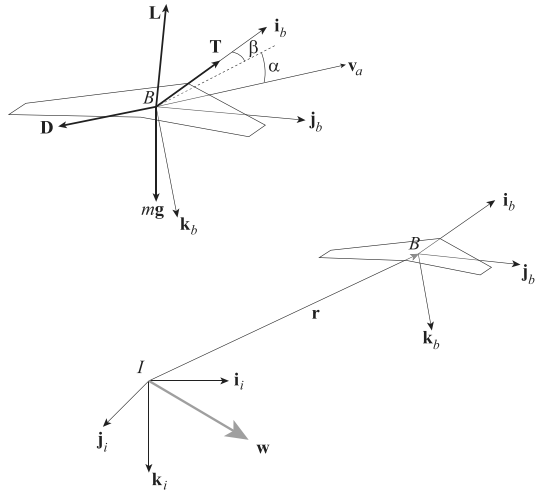

Fig. 1 Reference frames. The upper left image shows forces acting on the vehicle.

Using a standard body-fixed coordinate frame with air-mass-relative velocity $\mathbf{v}_a$ having components u, v, and w in the body $\mathbf{i}_b$, $\mathbf{j}_b$, and $\mathbf{k}_b$ directions, respectively, the velocity of the aircraft in the inertial frame is

$$\dot{\mathbf{r}} = \mathbf{v}_a + \mathbf{w} \tag{6}$$

Hence,

$$\ddot{\mathbf{r}} = \frac{\mathrm{d}}{\mathrm{d}t}\mathbf{v}_a + \frac{\mathrm{d}}{\mathrm{d}t}\mathbf{w} \tag{7}$$

where

$$\frac{\mathrm{d}}{\mathrm{d}t}\mathbf{v}_a = \begin{bmatrix} \dot{u} \\ \dot{v} \\ \dot{w} \end{bmatrix} + \boldsymbol{\omega} \times \mathbf{v}_a \tag{8}$$

Note that coordinate frames in Eq. (6) have not yet been specified: for convenience, the inertial frame I is used for $\mathbf{w}$, while the body-fixed frame is used for $\mathbf{v}_a$.

Substituting $\boldsymbol{\omega} = [\,p \quad q \quad r\,]^T$ (the angular velocity expressed in the body frame),

$$\mathbf{X} + \mathbf{Y} + \mathbf{Z} + m\mathbf{g} = m\Big[(\dot{u} + qw - rv)\mathbf{i}_b + (\dot{v} + ru - pw)\mathbf{j}_b + (\dot{w} + pv - qu)\mathbf{k}_b + \frac{\mathrm{d}}{\mathrm{d}t}\mathbf{w}\Big] \tag{9}$$

where $\mathbf{X}$, $\mathbf{Y}$, and $\mathbf{Z}$ are aerodynamic forces in the body i, $\mathbf{j}$, and $\mathbf{k}$ directions, respectively (these are functions of thrust, drag, and lift) and $m\mathbf{g}$ is the force due to gravity.

The vector of wind accelerations $\frac{\mathrm{d}}{\mathrm{d}t}\mathbf{w}$ is expressed in the inertial frame. Using a direction cosine matrix $\mathbf{T}$, which transforms a vector expressed in the inertial frame to a vector expressed in the body frame,

$$\mathbf{T} = \begin{bmatrix} \cos\theta\cos\psi & \cos\theta\sin\psi & -\sin\theta \\ \sin\phi\sin\theta\cos\psi - \cos\phi\sin\psi & \sin\phi\sin\theta\sin\psi + \cos\phi\cos\psi & \sin\phi\cos\theta \\ \cos\phi\sin\theta\cos\psi + \sin\phi\sin\psi & \cos\phi\sin\theta\sin\psi - \sin\phi\cos\psi & \cos\phi\cos\theta \end{bmatrix} \tag{10}$$

B. Vehicle Dynamics and Kinematics

Equations of motion of a flight vehicle in turbulent conditions are briefly derived. Consider an aircraft located at $\mathbf{r}$ in an inertial frame I, where $\mathbf{i}_i$, $\mathbf{j}_i$, and $\mathbf{k}_i$ define orthogonal unit vectors (see Fig. 1).

the body-axis accelerations with respect to the surrounding air are

$$\dot{u} = \frac{X}{m} - g\sin\theta - qw + rv - \dot{w}_{i,x}\cos\theta\cos\psi - \dot{w}_{i,y}\cos\theta\sin\psi + \dot{w}_{i,z}\sin\theta \tag{11}$$

$$\dot{v} = \frac{Y}{m} + g\sin\phi\cos\theta + pw - ru - \dot{w}_{i,x}(\sin\phi\sin\theta\cos\psi - \cos\phi\sin\psi) - \dot{w}_{i,y}(\sin\phi\sin\theta\sin\psi + \cos\phi\cos\psi) - \dot{w}_{i,z}\sin\phi\cos\theta \tag{12}$$

$$\dot{w} = \frac{Z}{m} + g\cos\phi\cos\theta + qu - pv - \dot{w}_{i,x}(\cos\phi\sin\theta\cos\psi + \sin\phi\sin\psi) - \dot{w}_{i,y}(\cos\phi\sin\theta\sin\psi - \sin\phi\cos\psi) - \dot{w}_{i,z}\cos\phi\cos\theta \tag{13}$$

Here, $\dot{w}_{i,(\cdot)}$ denotes the rate of change of a component of the wind velocity expressed in the inertial frame.

Given the vehicle dynamics in Eqs. (11–13), expressions for aerodynamic forces are required. Here, linearized expressions for forces and moments are used, so that [16]

$$X = X_0 + X_u\Delta u + X_w\Delta w + X_c \tag{14}$$

$$Y = Y_0 + Y_v v + Y_p(p - p_w) + Y_r(r - r_w) + Y_c \tag{15}$$

$$Z = Z_0 + Z_u\Delta u + Z_w\Delta w + Z_{\dot{w}}\dot{w} + Z_q(q - q_w) + Z_c \tag{16}$$

Stability and control derivatives are vehicle dependent. Except for $Z_{\dot{w}}$ derivatives, with respect to rate of change of motion, variables are neglected since they are typically small [16,17].

Finally, aircraft kinematics with respect to the Earth are

$$\begin{bmatrix}\dot{x}\\ \dot{y}\\ \dot{z}\end{bmatrix} = \mathbf{T}^{-1}\begin{bmatrix}u\\ v\\ w\end{bmatrix} + \begin{bmatrix}w_{i,x}\\ w_{i,y}\\ w_{i,z}\end{bmatrix} \tag{17}$$

where $\dot{x}$, $\dot{y}$, and $\dot{z}$ are the components of aircraft velocity with respect to the Earth in the Earth-fixed (i.e., inertial) reference frame; $\mathbf{T}$ is the direction cosine matrix [Eq. (10)]; u, v, and w are components of the aircraft velocity with respect to the air mass expressed in the body frame; and $w_{i,x}$, $w_{i,y}$, and $w_{i,z}$ are the components of the windspeed with respect to the Earth, expressed in the inertial reference frame.

C. Computing Wind from Vehicle Response

Rather than use a Kalman filter framework to estimate wind field in conjunction with aircraft states, one can compare measurements of aircraft motion with respect to the Earth with predictions of aircraft motion obtained from the dynamic model. The aircraft equations of motion can be separated into two parts: motion induced by the state and control inputs and motion induced by the wind field. Beginning with the equations for vehicle dynamics [Eqs. (11–13)], and kinematics [Eq. (17)],

$$\begin{bmatrix}\dot{x}\\ \dot{y}\\ \dot{z}\end{bmatrix} = \mathbf{T}^{-1}\begin{bmatrix}u\\ v\\ w\end{bmatrix} + \begin{bmatrix}w_{i,x}\\ w_{i,y}\\ w_{i,z}\end{bmatrix} \tag{18}$$

$$\begin{bmatrix}\dot{u}\\ \dot{v}\\ \dot{w}\end{bmatrix} = \begin{bmatrix}\frac{X}{m} - g\sin\theta - qw + rv\\ \frac{Y}{m} + g\sin\phi\cos\theta + pw - ru\\ \frac{Z}{m} + g\cos\phi\cos\theta + qu - pv\end{bmatrix} - \mathbf{T}\begin{bmatrix}\dot{w}_{i,x}\\ \dot{w}_{i,y}\\ \dot{w}_{i,z}\end{bmatrix} \tag{19}$$

Writing this compactly in discrete form using a forward Euler integration,

$$\mathbf{x}_k = \mathbf{x}_{k-1} + \Delta t f_u(\mathbf{x}_{k-1}, \mathbf{u}_{k-1}) + \Delta t\begin{bmatrix}\mathbf{I} & 0\\ 0 & -\mathbf{T}\end{bmatrix}\begin{bmatrix}\mathbf{w}_{k-1}\\ \dot{\mathbf{w}}_{k-1}\end{bmatrix} \tag{20}$$

where $x = [x \quad y \quad z \quad u \quad v \quad w]^T$ and f_u is the aircraft kinematic/dynamic model [i.e., the first terms on the right-hand side of Eqs. (18) and (19)]. Rearranging gives the wind field,

$$\begin{bmatrix}\mathbf{w}_{k-1}\\ \dot{\mathbf{w}}_{k-1}\end{bmatrix} = \frac{1}{\Delta t}\begin{bmatrix}\mathbf{I} & 0\\ 0 & -\mathbf{T}^{-1}\end{bmatrix}[\mathbf{x}_k - \mathbf{x}_{k-1} - \Delta t f_u(\mathbf{x}_{k-1}, \mathbf{u}_{k-1})] \tag{21}$$

This will compute the average value of wind velocity and wind acceleration over the time interval from $k-1$ to k. The quantity $\Delta t f_u(\mathbf{x}_{k-1}, \mathbf{u}_{k-1})$ is the prediction of the change in aircraft state over the time interval from $k-1$ to k while ignoring the direct effects of wind.

In principle, this approach is straightforward, since the state $\mathbf{x}$ can be measured directly (using GPS for position and air data sensors for airspeeds). In practice, however, it is not likely to give good results for two reasons. First, it relies on numerical differentiation of GPS position measurements: even with a wide-area augmentation system, GPS uncertainty is of the order of 3 m. While carrier phase differential GPS improves position accuracy to the order of centimeters, this is still significantly noisier than GPS velocity estimates. Second, aerodynamic forces are dependent on wind gradients through the $\dot{w}$, p, q, and r stability derivatives. If gradients are large, then predicted forces will be significantly different from actual forces, resulting in an error in f_u. Furthermore, this approach relies on an accurate dynamic model (this can be problematic for a small low-cost UAV) and accurate state estimates for computing a prediction of vehicle state.

D. Direct Computation of Wind Field

A better approach is to use GPS velocity (which is not obtained by numerically differentiating position measurements but by using the rates of change of pseudoranges) and measurements of vehicle acceleration. Combined with vehicle state information, this can be used to directly compute the wind field.

1. *Wind Velocity*

GPS provides a direct measurement of velocity with respect to the Earth, accurate to approximately 0.1 m/s (unaided, incorporating carrier phase differential GPS allows velocity measurements accurate to the order of millimeters per second) [18]. Thus, local air mass velocity components can be obtained directly from vehicle kinematics and the GPS velocity:

$$\begin{bmatrix}w_{i,x}\\ w_{i,y}\\ w_{i,z}\end{bmatrix} = \begin{bmatrix}\dot{x}\\ \dot{y}\\ \dot{z}\end{bmatrix}_{\text{GPS}} - \mathbf{T}^{-1}\begin{bmatrix}u\\ v\\ w\end{bmatrix} \tag{22}$$

This assumes that the autopilot module provides estimates of the components of airspeed and Euler angles (ϕ, θ, ψ). The effect of noise in GPS velocity measurements and in estimates of orientation and airspeed on the computed wind will be discussed later.

2. *Rate of Change of Wind Velocity (Wind Acceleration)*

The IMU provides measurements of body-axis acceleration with respect to the inertial frame and the gravity vector projected into the body frame:

$$\mathbf{z}_{\text{imu}} = \frac{\mathrm{d}}{\mathrm{d}t}\mathbf{v}_i - \mathbf{T}\mathbf{g} + \mathbf{b}_{\text{imu}} + \mathbf{n}_{\text{imu}} \tag{23}$$

where $\mathbf{v}_i$ is the velocity of the IMU with respect to the Earth expressed in the body frame, $\mathbf{b}_{\text{imu}}$ is the IMU bias (assumed known), and $\mathbf{n}_{\text{imu}}$ is zero-mean Gaussian random noise. Assuming the IMU is located at the aircraft center of gravity, substituting vehicle dynamics gives

$$\mathbf{z}_{\text{imu}} = \begin{bmatrix}a_{b,x}\\ a_{b,y}\\ a_{b,z}\end{bmatrix} = \begin{bmatrix}\dot{u} + \dot{w}_{b,x} + qw - rv + g\sin\theta\\ \dot{v} + \dot{w}_{b,y} + ru - pw - g\cos\theta\sin\phi\\ \dot{w} + \dot{w}_{b,z} + pv - qu - g\cos\theta\cos\phi\end{bmatrix} + \mathbf{b}_{\text{imu}} + \mathbf{n}_{\text{imu}} \tag{24}$$

Here, the wind acceleration is expressed in the body frame. Rearranging gives

$$\begin{bmatrix} \dot{w}_{b,x} \\ \dot{w}_{b,y} \\ \dot{w}_{b,z} \end{bmatrix} = \begin{bmatrix} a_{b,x} - qw + rv - g\sin\theta - b_{\text{imu},x} - \dot{u} \\ a_{b,y} - ru + pw + g\cos\theta\sin\phi - b_{\text{imu},y} - \dot{v} \\ a_{b,z} - pv + qu + g\cos\theta\cos\phi - b_{\text{imu},z} - \dot{w} \end{bmatrix} + \mathbf{n}_{\text{imu}} \tag{25}$$

where $b_{\text{imu},(\cdot)}$ denotes the components of the accelerometer bias.

There is no direct measurement of the rate of change of airspeed ($\dot{u}, \dot{v}, \dot{w}$) and no means of predicting the rate of change of airspeed. Hence, it must be computed by numerically differentiating measurements. This will be noisy, leading to potentially significant uncertainty in the computed values of rate of change of windspeed. It will also introduce a delay in the computation of wind acceleration. Here, a second-order numerical differentiation is used, so that

$$\begin{bmatrix} \dot{u} \\ \dot{v} \\ \dot{w} \end{bmatrix}_{k-1} = \frac{1}{2\Delta t} \begin{bmatrix} u_k - u_{k-2} \\ v_k - v_{k-2} \\ w_k - w_{k-2} \end{bmatrix} \tag{26}$$

This computes rate of change of airspeed at the previous time step. Substituting into Eq. (25) allows computation of the wind acceleration at the previous time step:

$$\begin{bmatrix} \dot{w}_{b,x} \\ \dot{w}_{b,y} \\ \dot{w}_{b,z} \end{bmatrix}_{k-1} = \begin{bmatrix} a_{b,x} - b_{\text{imu},x} - g\sin\theta \\ a_{b,y} - b_{\text{imu},y} + g\cos\theta\sin\phi \\ a_{b,z} - b_{\text{imu},z} + g\cos\theta\cos\phi \end{bmatrix}_{k-1} - \begin{bmatrix} qw - rv \\ pw - ru \\ qu - pv \end{bmatrix}_{k-1} - \frac{1}{2\Delta t} \begin{bmatrix} u_k - u_{k-2} \\ v_k - v_{k-2} \\ w_k - w_{k-2} \end{bmatrix} \tag{27}$$

This introduces a delay of one time step in computation of the wind acceleration. If the time step is short compared with vehicle and wind dynamics, then this will not have a large effect on the estimated wind. The error analysis presented later will show that errors in wind estimates can be explained by sensor noise; hence, the delay is likely to be insignificant.

The difference between this approach and that defined by Eq. (21) is in the use of inertial measurements rather than a vehicle dynamic model. Both approaches rely on numerically differentiating measurements of airspeed, but it is likely that measurements of acceleration will be more accurate than the predictions provided by a dynamic model.

Equations (22) and (27) together allow computation of the wind velocity (expressed in the inertial frame) and the wind acceleration as seen by the vehicle (expressed in the body frame). These can be used to compute velocity or trajectory commands for energy maximization, or other tasks such as disturbance minimization. It is useful, however, to determine the expected error in wind field estimates.

III. Error Analysis

The wind field computation is subject to errors resulting from several sources, with two main sources being measurement error and errors in vehicle state estimates. This section discusses and quantifies the magnitudes of the wind field estimate errors as functions of the magnitude of the measurement and state errors.

A. Wind Velocity Estimation

While the preceding computation was done in terms of airspeed body components u, v, and w, the results of the error analysis give intuitively more useful results when the wind computation is considered in terms of v_a, α, and β. Assuming wings-level flight,

$$w_{i,x} = \dot{x} - v_a\cos\gamma\cos\beta\cos\psi + v_a\cos\gamma\sin\beta\sin\psi \tag{28}$$

$$w_{i,y} = \dot{y} - v_a\cos\gamma\cos\beta\sin\psi - v_a\cos\gamma\sin\beta\cos\psi \tag{29}$$

$$w_{i,z} = \dot{z} - v_a\sin\gamma \tag{30}$$

where $\gamma = \theta - \alpha$, the flight-path angle with respect to the surrounding air mass.

Assuming that the errors in the measurements have a zero-mean Gaussian probability density, the error in the computed wind field can be determined by linearizing the preceding equations:

$$\mathbf{w} = h(\mathbf{z}) \approx h(\bar{\mathbf{z}}) + \mathbf{H}(\mathbf{z} - \bar{\mathbf{z}}) \tag{31}$$

Here, $\mathbf{z} = [\dot{x} \quad \dot{y} \quad \dot{z} \quad v_a \quad \gamma \quad \beta \quad \psi]^T$ and $\mathbf{H} = \nabla h$, the Jacobian of the wind computation equations with respect to the measurements $\mathbf{z}$. Assuming that the linearization of h is a good approximation over the range of uncertainty in $\mathbf{z}$, the error in estimated wind will have a zero-mean Gaussian probability density with covariance

$$\mathbf{\Sigma}_w = \mathbf{H}\mathbf{\Sigma}_z\mathbf{H}^T \tag{32}$$

where $\mathbf{\Sigma}_z$ is the covariance of the expected noise. If the measurement noise is uncorrelated, then

$$\mathbf{\Sigma}_z = \text{diag}(\sigma_{\dot{x}}^2 \quad \sigma_{\dot{y}}^2 \quad \sigma_{\dot{z}}^2 \quad \sigma_{v_a}^2 \quad \sigma_{\gamma}^2 \quad \sigma_{\beta}^2 \quad \sigma_{\psi}^2) \tag{33}$$

where $\sigma_{\gamma}^2 = \sigma_{\theta}^2 + \sigma_{\alpha}^2$.

The components of the wind error covariance are

$$\Sigma_w(1,1) = \sigma_{\dot{x}}^2 + \sigma_{v_a}^2\cos^2\gamma\cos^2(\beta+\psi) + \sigma_{\gamma}^2 v_a^2\sin^2\gamma\cos^2(\beta+\psi) + (\sigma_{\beta}^2 + \sigma_{\psi}^2)v_a^2\cos^2\gamma\sin^2(\beta+\psi) \tag{34}$$

$$\Sigma_w(1,2) = \sigma_{v_a}^2\cos^2\gamma\sin(\beta+\psi)\cos(\beta+\psi) + \sigma_{\gamma}^2 v_a^2\sin^2\gamma\sin(\beta+\psi)\cos(\beta+\psi) - (\sigma_{\beta}^2 + \sigma_{\psi}^2)v_a^2\cos^2\gamma\sin(\beta+\psi)\cos(\beta+\psi) \tag{35}$$

$$\Sigma_w(1,3) = -\sigma_{v_a}^2\sin\gamma\cos\gamma\cos(\beta+\psi) + \sigma_{\gamma}^2 v_a^2\sin\gamma\cos\gamma\cos(\beta+\psi) \tag{36}$$

$$\Sigma_w(2,2) = \sigma_{\dot{y}}^2 + \sigma_{v_a}^2\cos^2\gamma\sin^2(\beta+\psi) + \sigma_{\gamma}^2 v_a^2\sin^2\gamma\sin^2(\beta+\psi) + (\sigma_{\beta}^2 + \sigma_{\psi}^2)v_a^2\cos^2\gamma\cos^2(\beta+\psi) \tag{37}$$

$$\Sigma_w(2,3) = -\sigma_{v_a}^2\sin\gamma\cos\gamma\sin(\beta+\psi) + \sigma_{\gamma}^2 v_a^2\sin\gamma\cos\gamma\sin(\beta+\psi) \tag{38}$$

$$\Sigma_w(3,3) = \sigma_{\dot{z}}^2 + \sigma_{v_a}^2\sin^2\gamma + \sigma_{\gamma}^2 v_a^2\cos^2\gamma \tag{39}$$

The error covariance is symmetric, and offdiagonal terms represent correlation in the estimate error between components of the estimated wind. Correlation between the vertical and horizontal components (the 1, 3 and 2, 3 terms) can be removed by flying at $\gamma = 0$ (i.e., horizontal with respect to the surrounding air mass). Note that this is only possible during powered flight or during an unsteady glide: a steady, trimmed glide will always result in the aircraft descending in relation to the surrounding air mass. Correlation between horizontal components is removed by flying at $\beta + \psi = 0$, 90, 180, and 270°.

A measure of total error in the wind estimate is the trace of the covariance matrix:

$$e^2 = \text{Tr}\mathbf{\Sigma}_w = \sigma_{\dot{x}}^2 + \sigma_{\dot{y}}^2 + \sigma_{\dot{z}}^2 + \sigma_{v_a}^2 + \sigma_{\gamma}^2 v_a^2 + (\sigma_{\beta}^2 + \sigma_{\psi}^2)v_a^2\cos^2\gamma \tag{40}$$

Assuming that the flight-path angle γ is small, minimizing the total error implies flying at low airspeed. Indeed, minimum error will result from flying at zero airspeed, i.e., using a neutrally buoyant balloon.

In practice, the noise in the GPS velocity measurements will be correlated, but this will not affect the trace of the wind error covariance: it will add the GPS error correlation terms to the offdiagonal elements of $\mathbf{\Sigma}_w$.

When the flight-path angle is small, $\cos^2\gamma \approx 1$ and

$$e^2 = \sigma_{\dot{x}}^2 + \sigma_{\dot{y}}^2 + \sigma_{\dot{z}}^2 + \sigma_{v_a}^2 + v_a^2(\sigma_\gamma^2 + \sigma_\beta^2 + \sigma_\psi^2) = \sigma_{\dot{x}}^2 + \sigma_{\dot{y}}^2 + \sigma_{\dot{z}}^2 + \sigma_{v_a}^2 + v_a^2(\sigma_\theta^2 + \sigma_\alpha^2 + \sigma_\beta^2 + \sigma_\psi^2) \tag{41}$$

Since $\gamma = \theta - \alpha$, $\sigma_\gamma^2 = \sigma_\theta^2 + \sigma_\alpha^2$.

For unaided GPS, the standard deviation of the velocity error is approximately 0.1 m/s. This can be reduced with carrier phase differential GPS to the order of millimeters per second. Assuming that airspeed can be measured to an accuracy of 0.2 m/s (0.4 kt) and angles can be measured to an accuracy of 1°, the unaided value of estimation error is approximately $e^2 = 0.07 + 0.0012v_a^2$. Under these conditions, the angle-related errors equal the speed-measurement errors when airspeed is 7.58 m/s, and the total expected error at this speed is 0.37 m/s. When airspeed is 16 m/s, the expected error in computed windspeed is $e = 0.61$ m/s. If carrier phase differential GPS is used (assuming velocity error is 5 mm/s), the expected error is $e^2 = 0.0401 + 0.0012v_a^2$, leading to a predicted error of 0.59 m/s. This improvement is not significant: critical parameters in reducing windspeed estimate errors are the noise in measurements of airspeed and angles and flying at low airspeed.

B. Rate of Change of Wind Velocity Estimation

The Jacobian of $\dot{\mathbf{w}}$ with respect to measurements and states is obtained from Eq. (27):

$$\mathbf{H}_{\dot{\mathbf{w}}} = \begin{bmatrix} 1 & 0 & 0 & 0 & -g\cos\theta & -\frac{1}{\Delta t} & r & -q & 0 & -w & v \\ 0 & 1 & 0 & g\cos\theta\cos\phi & -g\sin\theta\sin\phi & r & -\frac{1}{\Delta t} & -p & -w & 0 & u \\ 0 & 0 & 1 & -g\cos\theta\sin\phi & -g\sin\theta\cos\phi & -q & p & -\frac{1}{\Delta t} & v & -u & 0 \end{bmatrix} \tag{42}$$

The covariance of the expected error in the wind acceleration estimate is

$$\mathbf{\Sigma}_{\dot{w}} = \mathbf{H}_{\dot{\mathbf{w}}}\mathbf{\Sigma}_x\mathbf{H}_{\dot{\mathbf{w}}}^T \tag{43}$$

where (for uncorrelated measurement noise)

$$\mathbf{\Sigma}_x = \mathrm{diag}(\sigma_{a_x}^2 \quad \sigma_{a_y}^2 \quad \sigma_{a_z}^2 \quad \sigma_\phi^2 \quad \sigma_\theta^2 \quad \sigma_u^2 \quad \sigma_v^2 \quad \sigma_w^2 \quad \sigma_p^2 \quad \sigma_q^2 \quad \sigma_r^2) \tag{44}$$

The square of the magnitude of the expected error is the trace of the covariance matrix:

$$\begin{aligned} e_{\dot{w}}^2 = \mathrm{Tr}\mathbf{\Sigma}_{\dot{w}} &= \sigma_{a_x}^2 + \sigma_{a_y}^2 + \sigma_{a_z}^2 + g^2\cos^2\theta\sigma_\phi^2 + g^2\sigma_\theta^2 \\ &+ \left(\frac{1}{\Delta t^2} + r^2 + q^2\right)\sigma_u^2 + \left(\frac{1}{\Delta t^2} + r^2 + p^2\right)\sigma_v^2 \\ &+ \left(\frac{1}{\Delta t^2} + p^2 + q^2\right)\sigma_w^2 + (w^2 + v^2)\sigma_p^2 + (w^2 + u^2)\sigma_q^2 \\ &+ (u^2 + v^2)\sigma_r^2 \end{aligned} \tag{45}$$

A major contributor to error is the numerical differentiation of the airspeed measurements (reflected in the $\sigma_{(u,v,w)}^2/\Delta t^2$ terms). The contribution of noise in angular rate measurements can be reduced by flying at low airspeed. Noise in the pitch and bank angles results in uncertainty of the projection of gravity into the body frame.

C. Smoothing/Filtering the Estimates

It is clear that estimates of windspeed and wind acceleration can be quite noisy. One approach to reducing noise is a smoothing filter such as a moving average. Clearly, filter length must be chosen carefully to reduce noise without causing too much lag in the estimates. Hand tuning found that a 10-step moving average significantly reduced noise in the wind estimates without greatly affecting lag.

D. Further Minimizing the Sensor Suite

It is difficult to carry a significant suite of sensors on a small (less than 4 ft wing span) vehicle. A possible low-cost low-impact sensor suite consists of an airspeed sensor, GPS, and magnetic compass. Moreover, this same suite can be used to produce a wind logging device that can be installed on sailplanes with minimal impact to measure wind fields during flight.

During steady flight, angle of attack typically varies between zero and approximately 8° (depending on airspeed). Sideslip is typically zero during cruise. A naive approach is to assume $\alpha = 4°$ with standard deviation 2° and $\beta = 0°$ with standard deviation 2°, so that the flight-path angle with respect to the air is $\gamma = \theta - 4°$ with variance $\sigma_\gamma^2 = 2 + \sigma_\theta^2$. At flight speeds typical of small UAVs (10 to 20 m/s), and assuming the remaining angles can be measured to an accuracy of 1°, the expected error in estimated windspeed will be between 0.61 and 1.14 m/s. With this reduced sensor suite, it will not be possible to compute the rates of change of windspeed.

IV. Simulation and Discussion

To assess the effectiveness of the proposed approach, both three-degree-of-freedom (3-DOF) and six-degree-of-freedom (6-DOF) simulations were conducted. The aircraft model is a small autonomous glider flying at approximately 16 m/s. A state feedback controller regulates states to maintain trimmed flight at best L/D. Note that the only control input is elevator deflection. An onboard autopilot module is assumed to provide measurements of position and Earth-relative velocity via GPS and estimates of airspeed and orientation. Measurements of body angular rates are provided by the autopilot module via its rate gyros. Assumed measurement noise and estimate uncertainties are given in Table 1. The autopilot is assumed to provide these data at a rate of 50 Hz. Under the conditions defined in Table 1, the expected error in wind velocity estimation at 16 m/s airspeed is 0.37 m/s for 3-DOF simulations and 0.46 m/s for 6-DOF simulations [Eq. (41)].

A. Gust Field Definition

Gust fields are modeled using a frozen Dryden turbulence model. Air mass motion is thus represented as a sum of sinusoids:

$$w_{(\cdot)} = w_{(\cdot),0} + \sum_{n=1}^{N} a_{(\cdot),n}\sin(\Omega_{(\cdot),n}s + \varphi_{(\cdot),n}) \tag{46}$$

where $(\cdot)$ denotes a component (either u or w for longitudinal or vertical gusts, respectively) and s is motion along the flight path. Random values of $\varphi_{(\cdot),n}$ simulate the random process, and the choice of coefficients $a_{(\cdot),n}$ defines the power spectral density. For a Dryden gust field, the power spectral density is defined as [15]

$$\Phi_u(\Omega) = \sigma_u^2\frac{2L_u}{\pi}\frac{1}{1 + (L_u\Omega)^2} \tag{47}$$

$$\Phi_w(\Omega) = \sigma_w^2\frac{L_w}{\pi}\frac{1 + 3(L_w\Omega)^2}{(1 + (L_w\Omega)^2)^2} \tag{48}$$

Table 1 Measurement noise and estimate uncertainties for simulations

Parameter	Source	Variable	1σ noise/uncertainty
Position	GPS measurement via autopilot	x, y, z	3 m
Orientation	State estimate from autopilot	ϕ, θ, ψ	$\sigma_\phi = \sigma_\psi = 0, \sigma_\theta = 1^\circ$
Airspeed	State estimate from autopilot	u, v, w	$\sigma_u = 0.2$ m/s, $\sigma_v = \sigma_w = 0.05$ m/s
Groundspeed	GPS measurement via autopilot	$\dot{x}, \dot{y}, \dot{z}$	0.1 m/s
Acceleration	IMU measurement via autopilot	$a_{x,b}, a_{y,b}, a_{z,b}$	0.1 m/s^2
Angular rate	IMU measurement via autopilot	p, q, r	0.01 rad/s

The Dryden gust spectrum is empirically determined from flight data with parameters defined in English units. For low altitudes (below 1000 ft, or 305 m), the length scale of the vertical gust is $L_w = h$ and the turbulence intensity is $\sigma_w = 0.1 w_{20}$, where w_{20} is the windspeed at 20 ft altitude (6 m). Horizontal gust length scale and intensity are related to the vertical gust scale and intensity by

$$\frac{L_u}{L_w} = \frac{1}{(0.177 + 0.000823h)^{1.2}} \tag{49}$$

$$\frac{\sigma_u}{\sigma_w} = \frac{1}{(0.177 + 0.000823h)^{0.4}} \tag{50}$$

where h is in feet.

The amplitude of a sinusoid in Eq. (46) is computed as [19]

$$a_n = \sqrt{\Delta\Omega_n \Phi(\Omega_n)} \tag{51}$$

Note that a sinusoidal gust field is represented by setting $N = 1$ and defining the amplitude at the desired frequency.

B. Dryden Gust Fields

Three-DOF simulations of flight through Dryden gust fields at an altitude of 50 m and $w_{20} = 10$ m/s were conducted to assess overall performance. A 500-run Monte Carlo simulation compares the predicted error with the actual error. Each run consists of a 60 s flight through a Dryden gust field, and a new gust field was generated for each run.

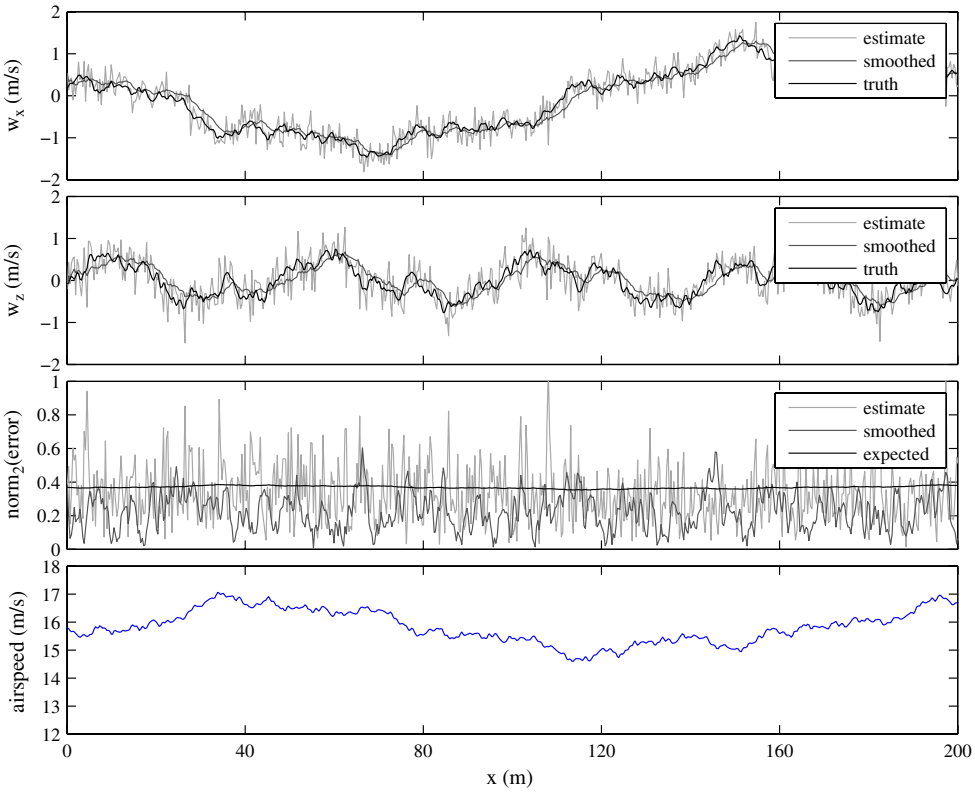

a) Detail of one run

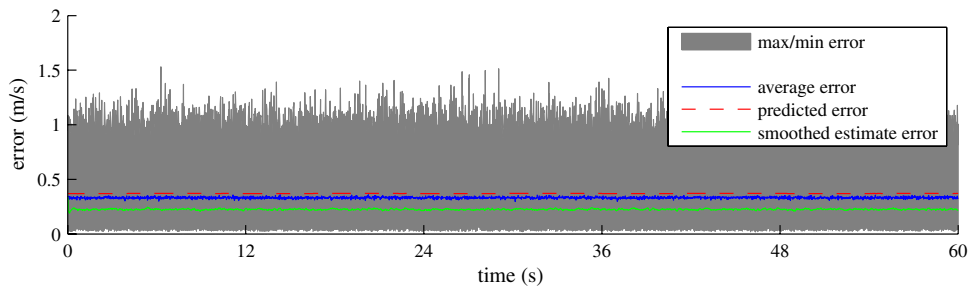

b) Monte Carlo simulation results

Fig. 2 Wind velocity estimation for 3-DOF Dryden wind field.

Results of wind velocity estimation are shown in Fig. 2. Detailed results of a single run (zoomed in to show a single wavelength of the x component of wind) are shown in Fig. 2a. The two upper plots of Fig. 2a show x and z components of wind field, estimated wind field, and smoothed estimated wind field. The lower plot shows the 2-norm of the error along with the expected error. For this run, the airspeed varies by about 1.5 m/s, not enough to have a significant influence on the estimation error.

Figure 2b shows overall results of the Monte Carlo simulation. Maximum error did not exceed 1.5 m/s, with the mean error of 0.33 m/s closely matching the predicted mean error of 0.37 m/s. Smoothing using a 10-step moving average reduced the mean error to 0.22 m/s.

Results of wind acceleration estimation are shown in Fig. 3. Detailed results of a single run (zoomed in to show a single wavelength of the x component of wind) are shown in Fig. 3a. The error in x component of wind acceleration is significantly larger than the z component. Expanding Eq. (43), and assuming longitudinal motion, the variance of the error in x and z components of wind acceleration are

$$\Sigma_{\dot{\mathbf{w}},xx} = \sigma_{a_x}^2 + g^2\sigma_\theta^2\cos^2\theta + \frac{1}{\Delta t^2}\sigma_u^2 + q^2\sigma_w^2 + w^2\sigma_q^2 \tag{52}$$

$$\Sigma_{\dot{\mathbf{w}},zz} = \sigma_{a_z}^2 + g^2\sigma_\theta^2\sin^2\theta + \frac{1}{\Delta t^2}\sigma_w^2 + q^2\sigma_u^2 + u^2\sigma_q^2 \tag{53}$$

These simulations have defined as σ_u four times larger than σ_w; hence, the standard deviation of the error in x acceleration estimates will be roughly four times larger than the w acceleration estimates.

Figure 3b shows the envelope of the 2-norm of the acceleration estimate error, the mean acceleration error, and the predicted acceleration error. The mean true error was 8.6 m/s^2, and the predicted error was 10.0 m/s^2. Smoothing reduced error to 4.33 m/s^2 at a cost of reducing the ability to follow changes in acceleration. An improved model for airspeed measurements would greatly improve estimation of wind acceleration.

C. Sinusoidal Gust Fields

Estimator performance in three-dimensional wind fields was assessed through simulations of flight through noisy sinusoidal gust fields.

Results of wind velocity estimation are shown in Fig. 4. Detailed results of a single run are shown in Fig. 4a. The three upper plots of Fig. 4a show x, y, and z components of wind field, estimated wind field, and smoothed estimated wind field. The lower plot shows the 2-norm of the error along with the expected error. For this run, the airspeed varies from 13.5 to 19.5 m/s, roughly in phase with increasing headwind (negative values of w_x), and this is enough that the effect of airspeed on estimation error can be seen. Increasing airspeed corresponds to increasing error in the estimated wind field, as predicted.

Figure 4b shows overall results of the Monte Carlo simulation. Maximum error did not exceed 1.5 m/s, with the mean error of 0.45 m/s closely matching the predicted mean error of 0.46 m/s.

Results of wind acceleration estimation are shown in Fig. 5. Detailed results of a single run are shown in Fig. 5a. The three upper plots of Fig. 5a show x, y, and z components of wind acceleration, estimated wind acceleration, and smoothed estimated wind

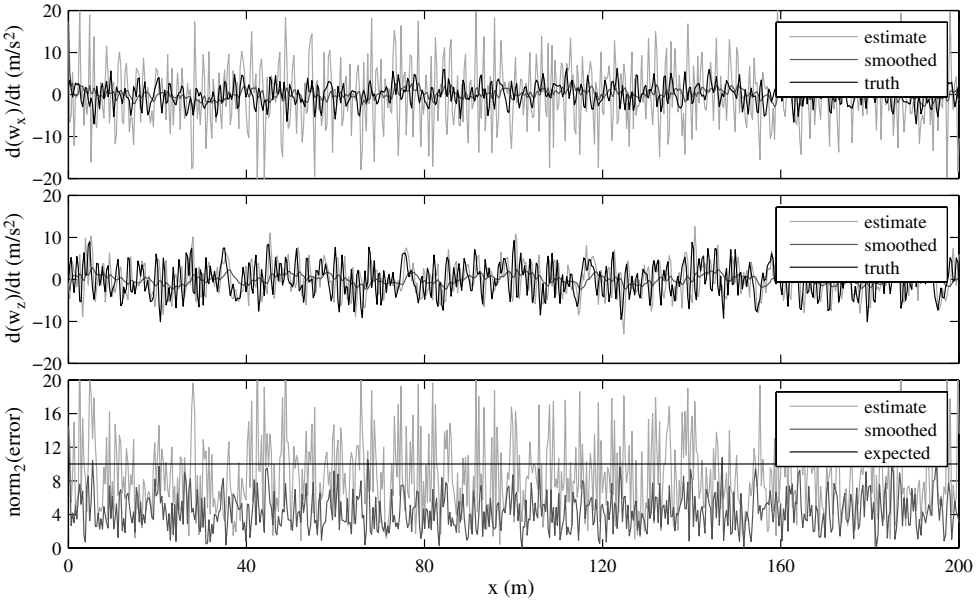

a) Detail of one run

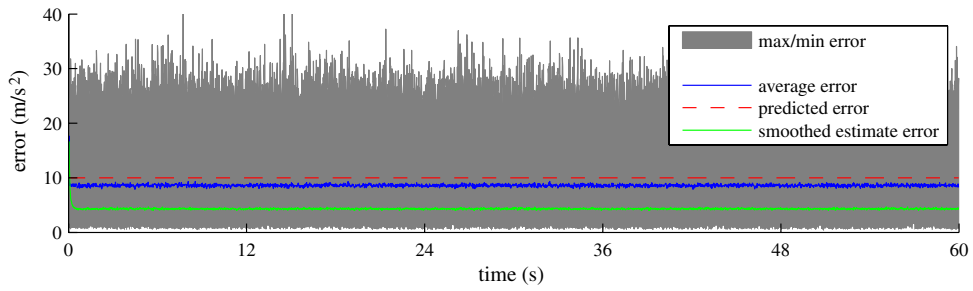

b) Monte Carlo simulation results

Fig. 3 Wind acceleration estimation for 3-DOF Dryden wind field.

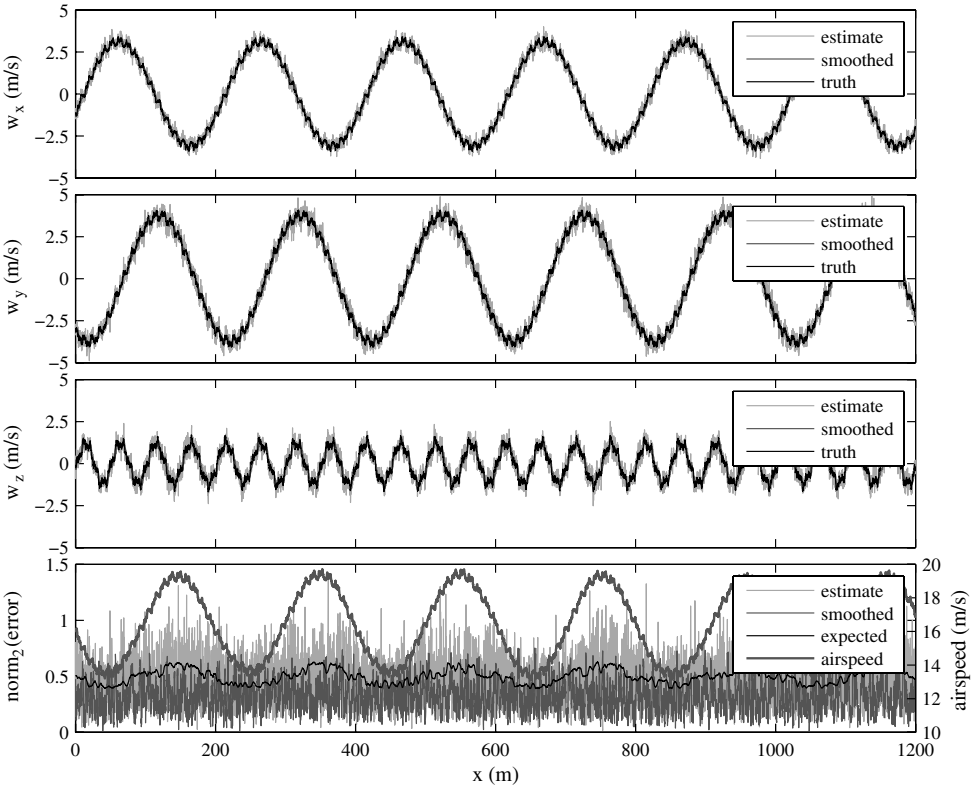

a) Detail

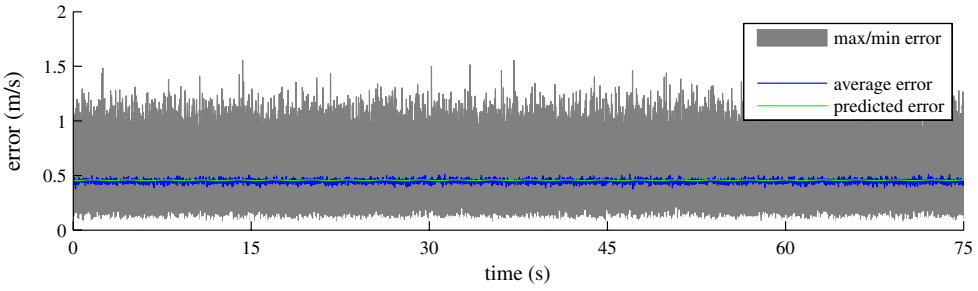

b) Monte Carlo simulations

Fig. 4 Six-DOF wind velocity estimation for noisy sinusoidal wind field.

acceleration. The lower plot shows the 2-norm of the error along with the expected error. Not surprisingly, estimates of wind acceleration are very noisy (due to the numerical differentiation of the airspeed measurement). Since the largest contributor to error is the numerical differentiation, the expected error is essentially constant at 13.8 m/s^2.

Figure 5b shows overall results of a Monte Carlo simulation. For the Monte Carlo simulation, the time step was set to 0.02 s, double the value for the detailed plot. The mean error is therefore half the value of the error in the detailed plot. The predicted mean error and the true mean error match very closely.

V. Wind Estimation and Energy Harvesting

Since earlier research has shown that energy harvesting from gusts is feasible when wind is known, an important question is the feasibility of energy harvesting when wind is not known. Simulations of longitudinal energy harvesting using a slight modification of a previously developed gust soaring control architecture along with the wind estimation algorithm presented here are discussed.

This architecture is shown in Fig. 6. In brief, measurements of airspeed, GPS velocity, orientation, acceleration, and angular rate are used to estimate the wind field. The components of windspeed are used to compute a state that maximizes the change in energy per unit of distance travelled, and a closed-loop controller attempts to follow these state commands. Here, the closed-loop control law is computed using linear quadratic regulator (LQR) synthesis, with vehicle dynamics linearized about steady trimmed flight at best L/D [20].

There is an important difference in the speed computation used here and that described earlier: wind gradients are not included in the computation of speed to fly. A brief investigation (not discussed here) showed that including wind gradients in the energy harvesting state computation for gust fields involving longitudinal as well as vertical gusts did not provide as large a performance gain as it did in fields involving only vertical gusts (even when winds were assumed known). This may be due to an incorrect choice of weight matrices $\mathbf{Q}$ and $\mathbf{R}$ in the LQR synthesis (matrices computed in earlier work for vertical-only gusts were used here rather than computing new values including the effects of longitudinal gusts [20]). However, this requires further investigation.

The vehicle considered is the RnR Products SB-XC, a 4.3 m wing span aircraft. Note that this aircraft is hand-launchable: both the author and other researchers have demonstrated hand launch [21,22]. Parameters are given in Table A1 and control saturation and state limits are given in Table A2. The controller gain used for all cases was [20]

$$\mathbf{K} = [1.0106 \quad -0.0277 \quad 5.8082 \quad 0.5847] \tag{54}$$

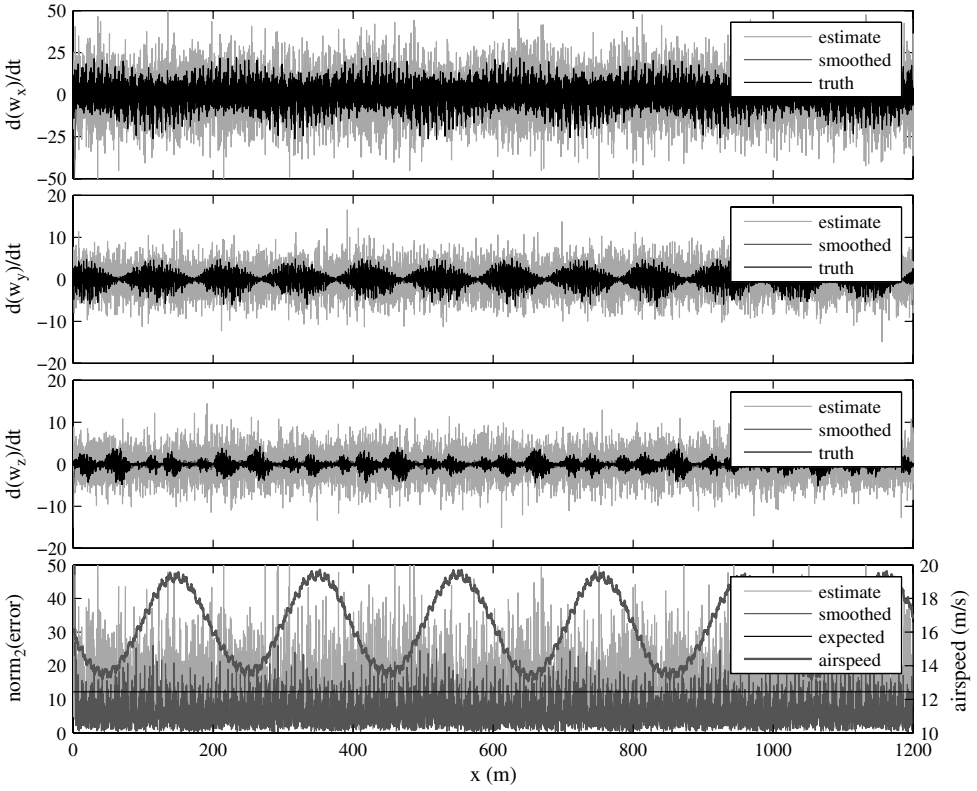

a) Detail

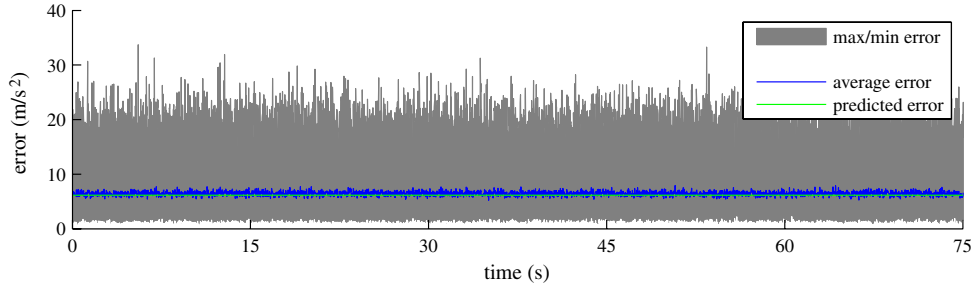

b) Monte Carlo simulations

Fig. 5 Six-DOF wind acceleration estimation for noisy sinusoidal wind field.

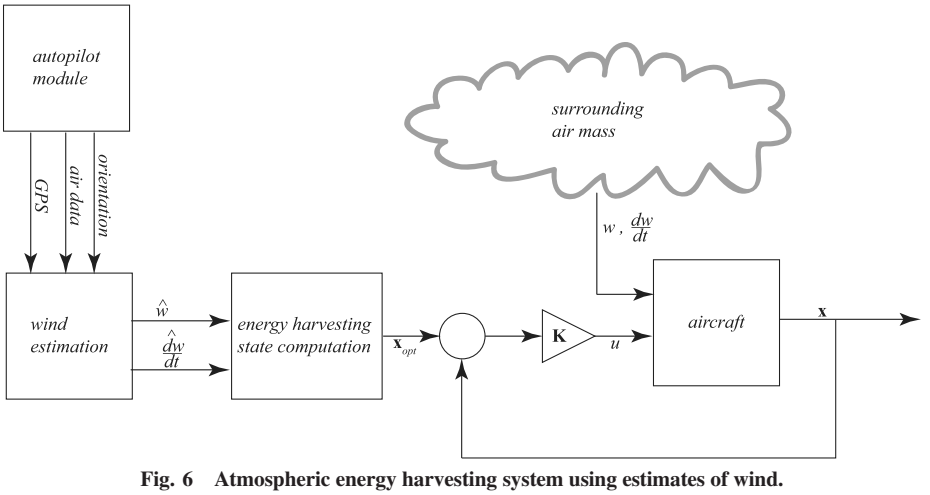

Fig. 6 Atmospheric energy harvesting system using estimates of wind.

Table 2 Gust field properties

Description	Altitude, m	L_u, m	L_w, m	σ_u, m/s	σ_w, m/s
Low altitude, light turbulence	50	200	50	1.06	0.7
Low altitude, moderate turbulence	50	200	50	2.12	1.4
Medium altitude, light turbulence	600	533	533	1.5	1.5
Medium altitude, moderate turbulence	600	533	533	3.0	3.0

Simulation result flights through four turbulence conditions are presented: low altitude, light turbulence; low altitude, moderate turbulence; medium altitude, light turbulence; and medium altitude, moderate turbulence. Properties of the gust fields are defined by MIL-F-8785C [15] and are summarized in Table 2. Note that medium altitude gust fields are isotropic, while at low altitude (below 1000 ft), both gust intensity and the fundamental length depends on direction. For each case, a Monte Carlo simulation of 50 runs was performed to assess flight performance using four controllers: 1) the constant airspeed flight controller; 2) the gust energy harvesting controller assuming known wind conditions; 3) the gust energy harvesting controller using estimated wind conditions; and 4) the gust energy harvesting controller using smoothed estimates. The constant speed flight controller uses the same gain matrix computed for gust energy harvesting; however, rather than attempting to follow state commands for optimal energy harvesting, it tracks the state that defines a trimmed glide at best L/D in still air ($v_a = 15.8$ m/s, $\theta = 0.7°$, and $\alpha = 2.8°$).

Each run consisted of 8 min of simulated flight through the gust field, resulting in approximately 7600 m of distance flown for each run. A new random gust field was generated for each of the 50 runs.

Results of all cases are summarized in Fig. 7. Figure 7a shows maximum, minimum, mean, and 1σ values of $\Delta e_{\text{tot}}/\Delta x$ (i.e., change in total energy over distance flown) for each control case over the 50 runs in each turbulence case. The dotted black line in the upper plot of Fig.7a shows de/dx for a steady glide at best L/D in still air. The lower plot of Fig. 7a shows the average (over all runs) of the root-mean-square elevator deflection for each controller (a measure of the amount of control required).

The difference in energy harvesting using known versus estimated wind is slight (the plots lie essentially on top of each other). Steadily increasing improvement over the baseline (constant speed) case is visible. In fact, the medium altitude cases show that many of the gust fields actually result in net energy gain.

However, a clear difference is visible in the root-mean-square elevator deflection, with the use of wind estimates greatly increasing required control (Fig. 7a, lower plot). Using smoothed wind estimates reduces root-mean-square elevator deflection to the level observed for energy harvesting using known wind; however, it does not significantly reduce the energy harvested.

The difference in energy change between the energy harvesting controller and a constant airspeed controller is shown in Fig. 7b. The gust energy harvesting controller shows better performance for all runs, with the level of improvement increasing as the turbulence intensity increases.

Detailed results for each turbulence condition are shown in Figs. 8–11. Figures 8a, 9a, 10a, and 11a show single representative runs, and Figs. 8b, 9b, 10b, and 11b show the mean total energy versus distance (averaged over all runs). The dotted black lines in Figs. 8b, 9b, 10b, and 11b show energy change versus distance for steady glide in zero wind.

A general conclusion is that the constant speed controller flies too slowly in regions of unfavorable wind (downward or headwind) and too fast in regions of favorable wind (upward or tailwind). Thus, too much time is spent in unfavorable conditions and not enough time is spent in favorable conditions. This is magnified in the medium altitude cases, where the length scale of turbulence is larger. Second, significantly more elevator deflection is required at lower altitudes for all controllers. This is most likely due to the shorter scales of turbulence.

VI. Conclusions

A method for estimating dynamic three-dimensional wind fields using a sensor suite typical of small UAVs has been presented. Analysis of the predicted error shows that the error in wind velocity estimates is dependent on vehicle airspeed and the error in wind acceleration is due in large part to noise in measurements of airspeed. Results of Monte Carlo simulations agree very closely with the predicted errors.

Simulations using realistic levels of noise and uncertainty show that wind velocity can be estimated to an accuracy of better than 0.5 m/s. Since the Earth-relative velocity of the vehicle can be measured quite accurately using GPS, the key to reducing this error

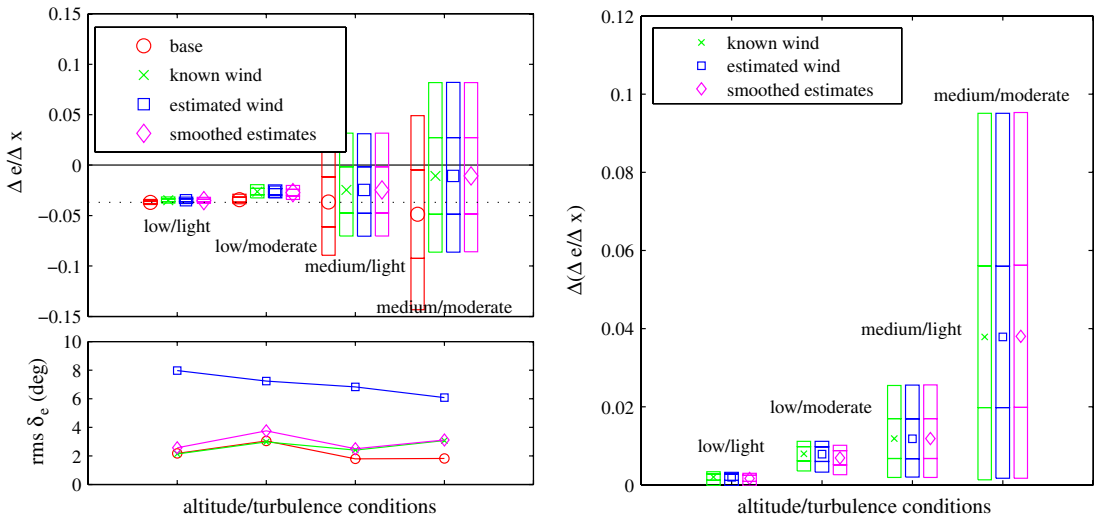

a) Energy change and control effort **b) Improvement in energy change over baseline**

Fig. 7 Summary of energy harvesting using estimated winds for all turbulence conditions.

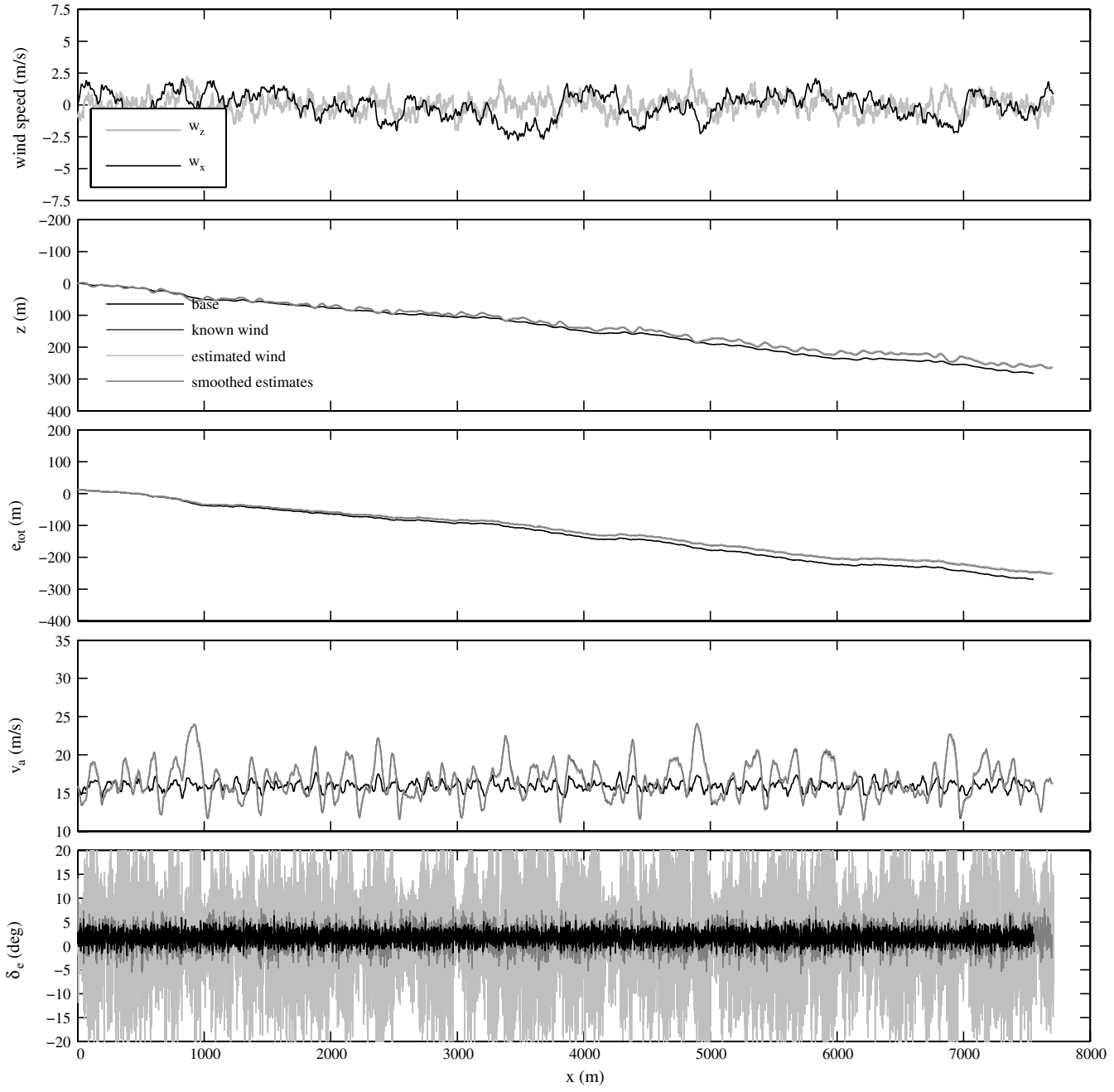

a) Single run detail

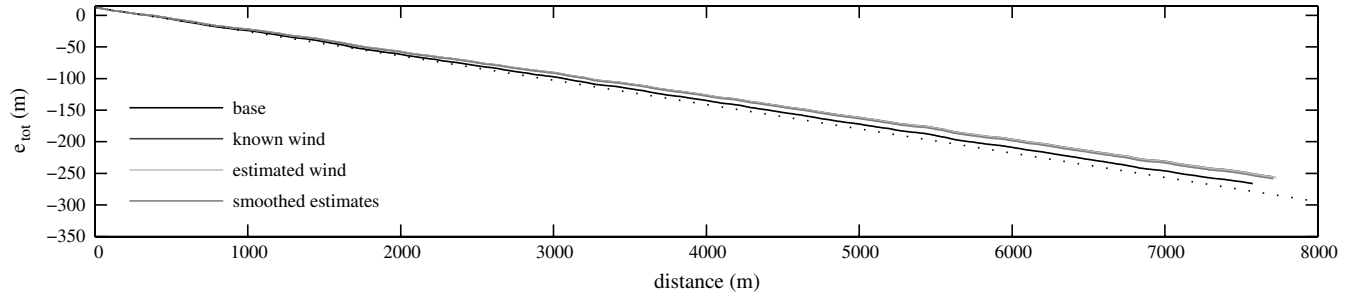

b) Mean total energy

Fig. 8 Performance comparison for flight through Dryden turbulence at low altitude, light intensity.

further is increasing the accuracy of airspeed measurements and increasing the accuracy of vehicle orientation measurements.

Simulations combining this wind field estimation algorithm with a gust energy harvesting controller showed that efficient energy harvesting is possible, even without perfect a priori knowledge of the wind field. The cost of using wind estimates lies in significantly increased control actuation, but this can be greatly reduced by smoothing the estimates using a moving average filter. This

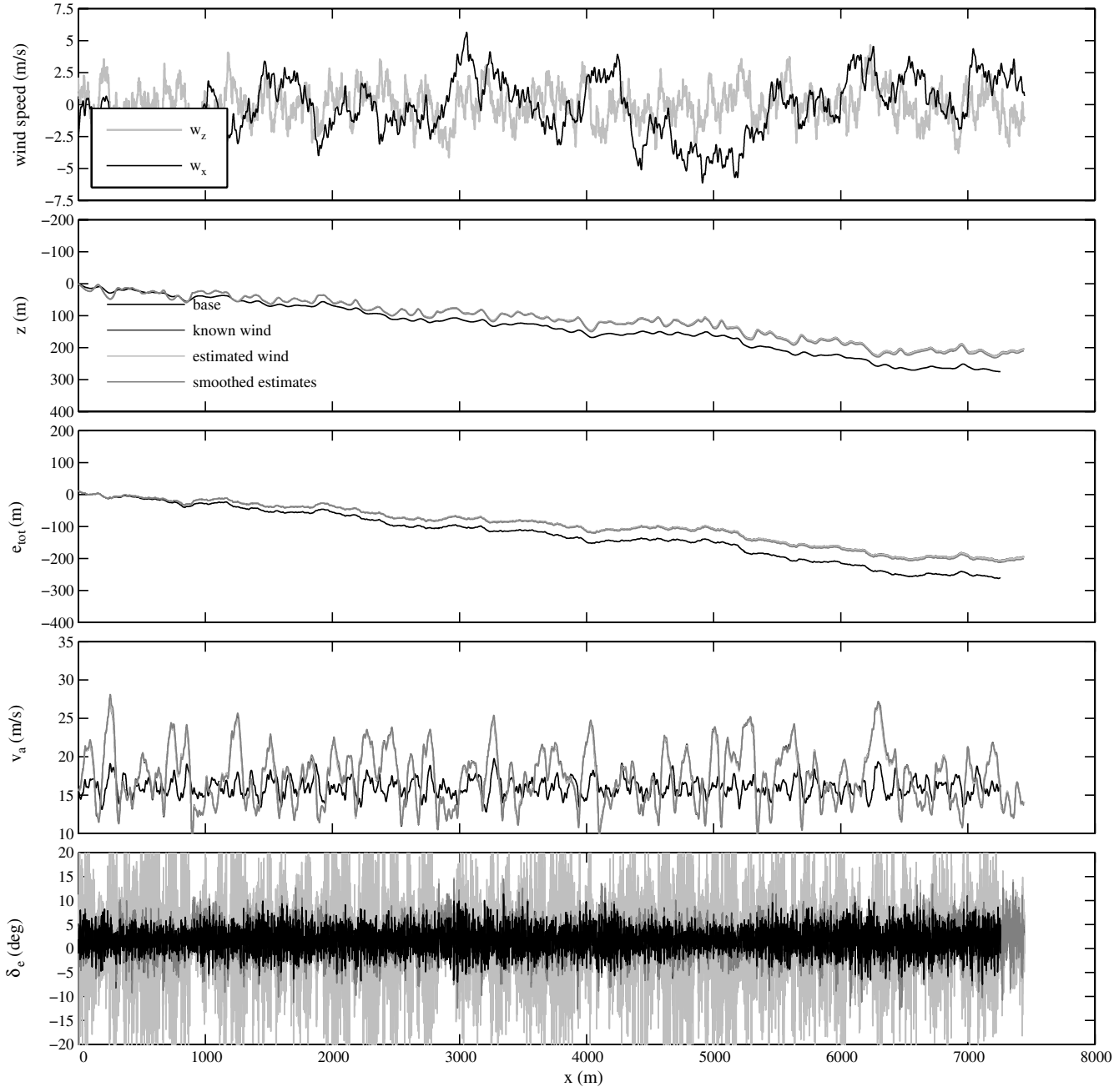

a) Single run detail

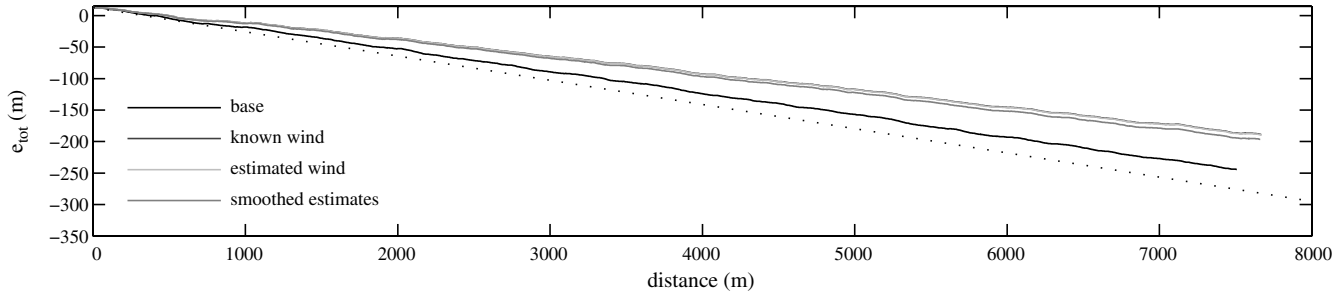

b) Mean total energy

Fig. 9 Performance comparison for flight through Dryden turbulence at low altitude, moderate intensity.

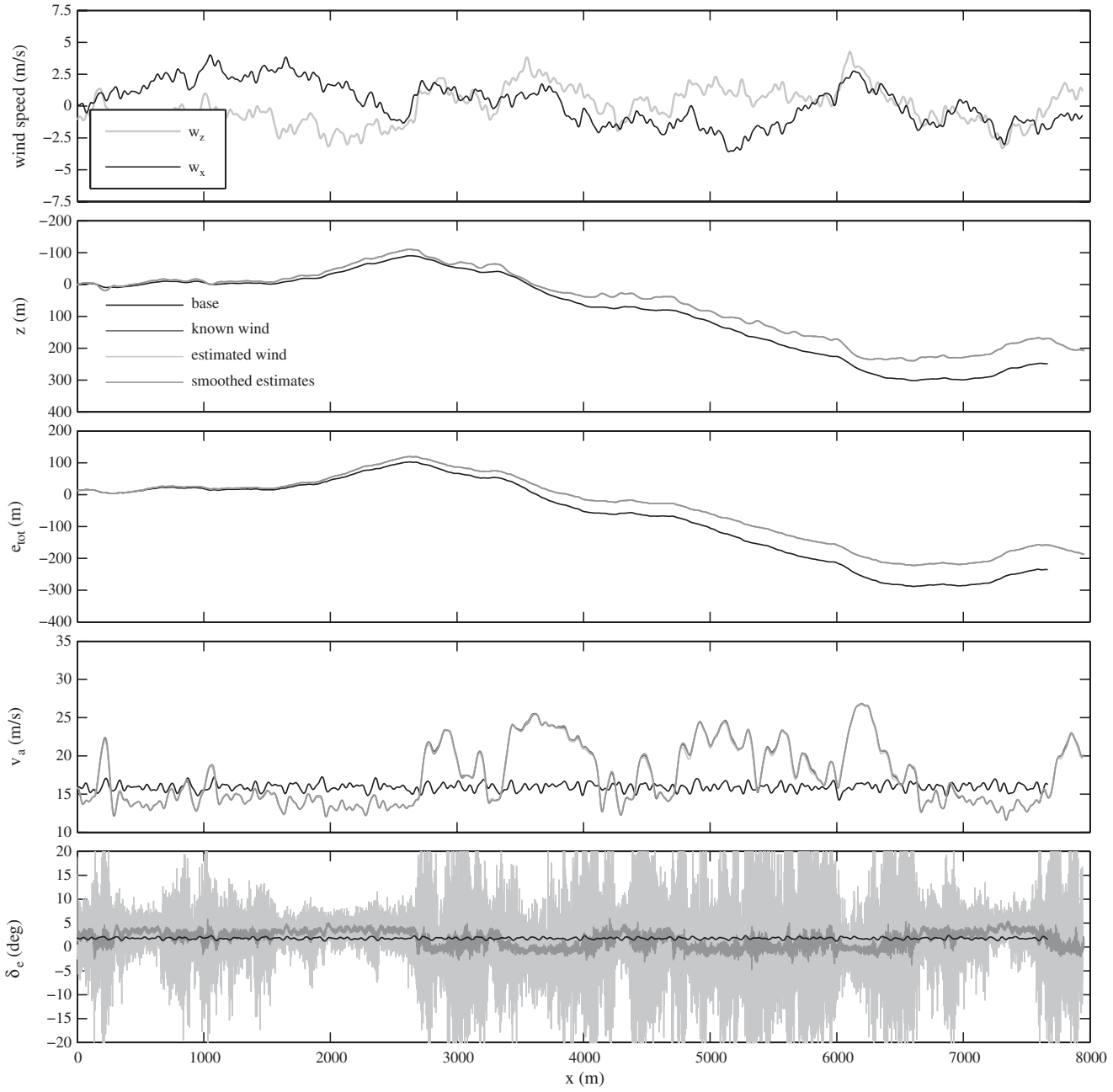

a) Single run detail

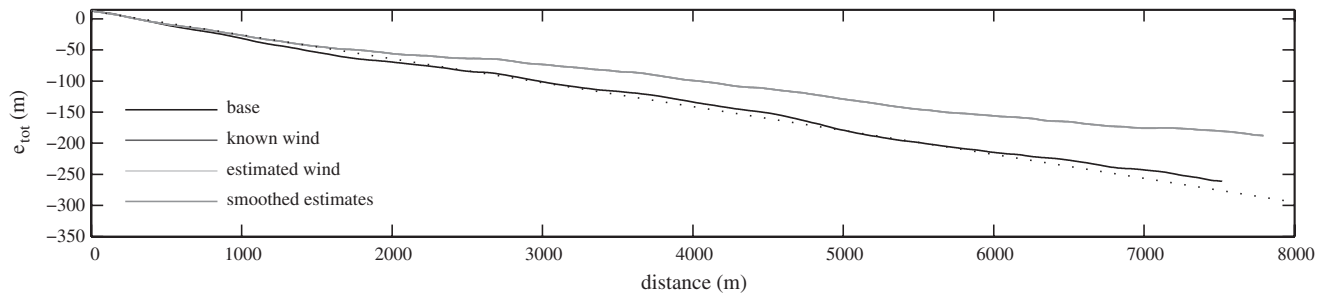

b) Mean total energy

Fig. 10 Performance comparison for flight through Dryden turbulence at medium altitude, light intensity.

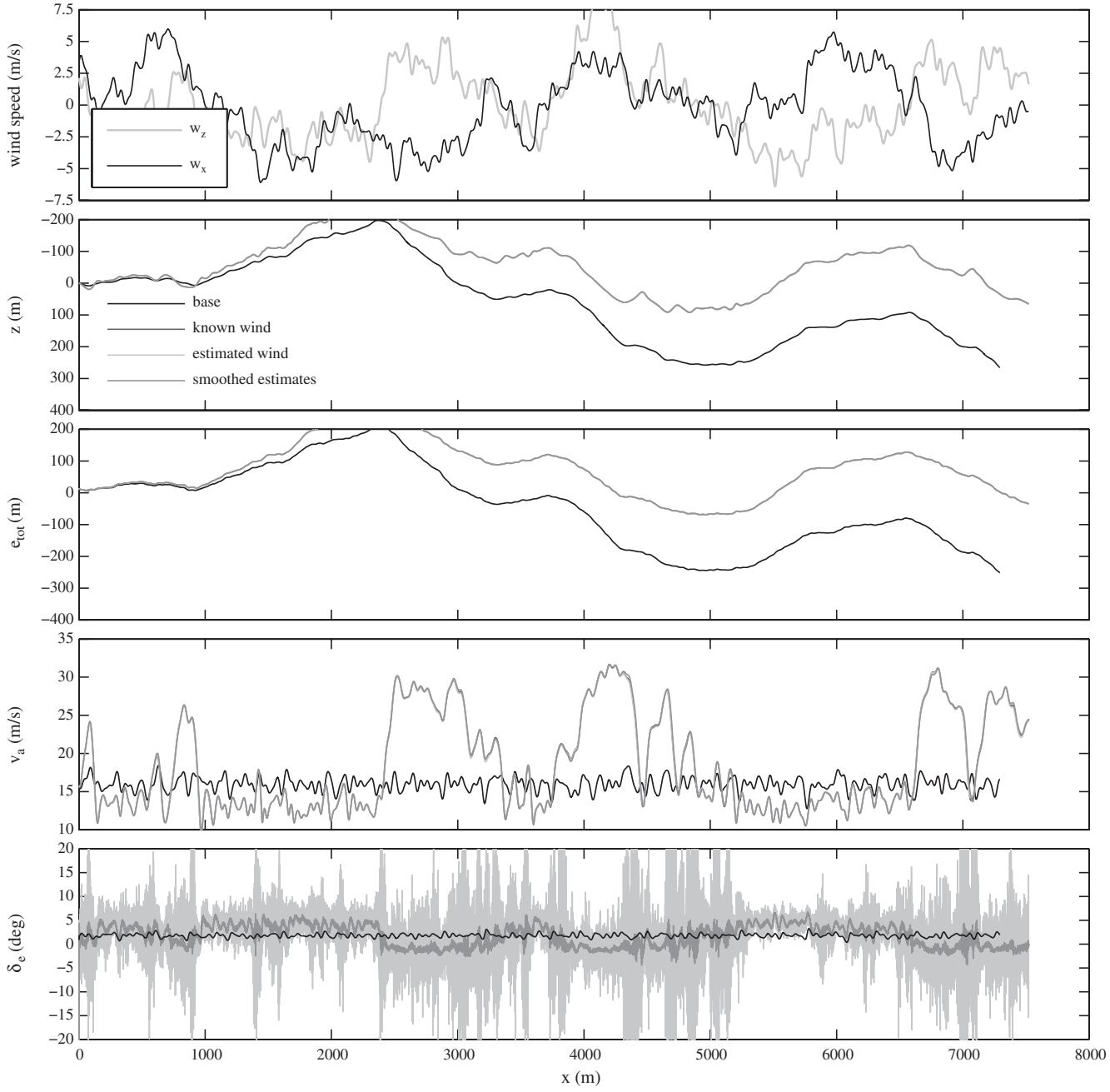

a) Single run detail

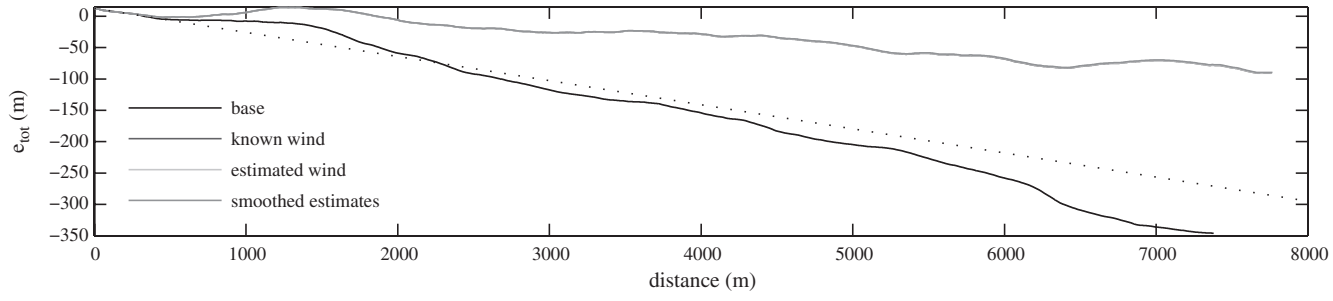

b) Mean total energy

Fig. 11 Performance comparison for flight through Dryden turbulence at medium altitude, moderate intensityd.

smoothing filter reduced control actuation to the level observed for flight through a priori known wind fields without significant effect on energy harvesting.

Appendix: Vehicle Properties

Table A1 Parameters for SB-XC glider

Variable	Value	Description
m	10 kg	Mass
b	4.34 m	Span
c	0.232 m	Mean aerodynamic chord
S	1 m^2	Wing area
I_{yy}	1.87 kg.m^2	Pitch moment of inertia
C_{L0}	0.37	
C_{L_α}	5.54/rad	
C_{L_Q}	−3.255 s/rad	
$C_{L_{\dot{\alpha}}}$	−0.651 s/rad	
$C_{L_{\delta_e}}$	−0.37/rad	
$C_{L_{\delta_f}}$	1.63/rad	
$f_{LD}(\varphi)$	$0.1723\varphi^4 - 0.3161\varphi^3 + 0.2397\varphi^2 - 0.0624\varphi + 0.0194$	$\varphi = C_{L0} + C_{L_\alpha}\alpha$
$C_{D_{\delta_e}}$	0/rad	
$C_{D_{\delta_f}}$	0.042/rad	
C_{m0}	0	
C_{m_α}	−1.02/rad	
C_{m_Q}	−14.6 s/rad	
$C_{m_{\delta_e}}$	1.6275/rad	
$C_{m_{\delta_f}}$	−0.254/rad	

Table A2 State limits and control saturation for SB-XC glider

State/control	Range	Description
θ	−45–45°	Pitch
v_a	11–35 m/s	Airspeed
α	2–12°	Angle of attack
Q	−999–999	Pitch rate
δ_e	−20–20°	Elevator deflection

Acknowledgments

This research was funded by the Office of Naval Research under Contract Number N00014-09-M-0307. The authors also thank Dan Kuehme for assistance in running simulations.

References

[1] Rayleigh, J. W. S., "The Soaring of Birds," *Nature*, Vol. 27, No. 701, 1883, pp. 534–535. doi:10.1038/027534a0

[2] Rayleigh, J. W. S., "The Sailing Flight of the Albatross," *Nature*, Vol. 40, No. 1019, 1889, p. 34. doi:10.1038/040034b0

[3] Pennycuick, C. J., "Gust Soaring as a Basis for the Flight of Petrels and Albatrosses (Procellariiformes)," *Avian Science*, Vol. 2, No. 1, 2002, pp. 1–12.

[4] Sachs, G., "Minimum Shear Wind Strength Required for Dynamic Soaring of Albatrosses," *Ibis*, Vol. 147, No. 1, 2005, pp. 1–10. doi:10.1111/j.1474-919x.2004.00295.x

[5] Lissaman, P. B. S., and Patel, C. K., "Neutral Energy Cycles for a Vehicle in Sinusoidal and Turbulent Vertical Gusts," 45th AIAA Aerospace Sciences Meeting and Exhibit, Reno, NV, AIAA Paper 2007-0863, Jan. 2007.

[6] Qi, Y. C., and Zhao, Y. J., "Energy-Efficient Trajectories of Unmanned Aerial Vehicles Flying Through Thermals," *Journal of Aerospace Engineering*, Vol. 18, No. 2, April 2005, pp. 84–92. doi:10.1061/(ASCE)0893-1321(2005)18:2(84)

[7] Langelaan, J. W., and Bramesfeld, G., "Gust Energy Extraction for Mini- and Micro–Uninhabited Aerial Vehicles," 46th AIAA Aerospace Sciences Meeting and Exhibit, AIAA Paper 2008-0223, Jan. 2008.

[8] Patel, C. K., *Energy Extraction from Atmospheric Turbulence to Improve Aircraft Performance*, VDM Verlag Dr. Müller, Saarbrüken, Germany, 2008.

[9] Watkins, S., Milbank, J., and Loxton, B. J., "Atmospheric Winds and the Implications for Microair Vehicles," *AIAA Journal*, Vol. 44, No. 11, Nov. 2006, pp. 2591–2600. doi:10.2514/1.22670

[10] Pachter, M., Ceccarelli, N., and Chandler, P. R., "Estimating MAV's Heading and the Wind Speed and Direction using GPS, Inertial and Air Speed Measurements," AIAA Guidance, Navigation and Control Conference, AIAA Paper 2008-6311, Aug. 2008.

[11] Rodriguez, A. F., Andersen, E., Bradley, J. F., and Taylor, C. N., "Wind Estimation Using an Optical Flow Sensor on a Miniature Air Vehicle," AIAA Guidance, Navigation and Control Conference, AIAA Paper 2007-6614, Aug. 2007.

[12] Myschik, S., Heller, M., Holzapfel, F., and Sachs, G., "Low-Cost Wind Measurement System for Small Aircraft," AIAA Guidance, Navigation and Control Conference, AIAA Paper 2004-5240, Aug. 2004.

[13] Myschik, S., and Sachs, G., "Flight Testing an Integrated Wind/Airdata and Navigation System for General Aviation Aircraft," AIAA Guidance, Navigation and Control Conference, AIAA Paper 2007-6796, Aug. 2007.

[14] de Divitiis, N., "Wind Estimation on a Lightweight Vertical Takeoff and Landing Uninhabited Vehicle," *Journal of Aircraft*, Vol. 40, No. 4, July–Aug. 2003, pp. 759–767. doi:10.2514/2.3155

[15] "Flying Qualities of Piloted Airplanes," U.S. Department of Defense TR MIL-F-8785C, Nov. 1980.

[16] Etkin, B., and Reid, L. D., *Dynamics of Flight: Stability and Control*, 3rd ed., Wiley, New York, 1996, Chap. 4.

[17] McCormick, B. W., *Aerodynamics, Aeronautics and Flight Mechanics*, 2nd ed., Wiley, Hoboken, NJ, 1995, Chap. 6.

[18] Misra, P., and Enge, P., *Global Positioning System: Signals, Measurements and Performance*, 2nd ed., Ganga-Jamuna Press, Lincoln, MA, 2006, Chap. 4.

[19] Hoblit, F. M., *Gust Loads on Aircraft: Concepts and Applications*, AIAA Education Series, AIAA, Reston, VA, 1988.

[20] Langelaan, J. W., "Gust Energy Extraction for Mini- and Micro-Uninhabited Aerial Vehicles," *Journal of Guidance, Control, and Dynamics*, Vol. 32, No. 2, March–April 2009, pp. 464–473. doi:10.2514/1.37735

[21] Allen, M. J., and Lin, V., "Guidance and Control of an Autonomous Soaring Vehicle with Flight Test Results," AIAA Aerospace Sciences Meeting and Exhibit, Reno, NV, AIAA Paper 2007-867, Jan. 2007.

[22] Anderson, K., Kaminer, I., and Jones, K. D., "Autonomous Soaring; Flight Test Results of a Thermal Centering Controller," AIAA Guidance, Navigation and Control Conference, Toronto, AIAA Paper 2010-8034, Aug. 2010.